Soft Matter

RSC Publishing

PAPER

View Article Online
View Journal | View Issue

Cite this: *Soft Matter*, 2013, **9**, 10729

Self-assembly of colloidal hematite cubes: a microradian X-ray diffraction exploration of sedimentary crystals†

Janne-Mieke Meijer,[a] Dmytro V. Byelov,[a] Laura Rossi,‡[a] Anatoly Snigirev,[b] Irina Snigireva,[b] Albert P. Philipse[a] and Andrei V. Petukhov*[a]

Received 4th June 2013
Accepted 12th September 2013

DOI: 10.1039/c3sm51553b

www.rsc.org/softmatter

The structure of spontaneously formed crystals in the sediments of colloidal hematite (α-Fe_2O_3) cubes is studied using microradian X-ray diffraction. The hematite cubes possess a superball shape and a permanent magnetic dipole moment, both influencing the self-assembly behaviour and inducing directionality in different ways. To control the inter-cube interactions, the cubes were dispersed in different solvents and/or coated with a silica layer and allowed to form sediments under the simultaneous effect of the gravitational field and an applied magnetic field. The microradian X-ray diffraction revealed that changing the double layer repulsion that opposes the magnetic and van der Waals attractions can induce short to long-range ordering in the fast sedimenting systems of the cubes. The presence of an external magnetic field during sedimentation induced the formation of a single crystal with long-range order that showed different symmetries, rectangular or hexagonal, close to the fluid–solid interface. The identified 3D crystal structure of both was found to have a body centred monoclinic lattice periodicity that rotates deeper in the sediment due to gravitational compression. This experimental structure differs from the expected crystal lattices determined by simulations and is most likely due to the effects of long-range repulsion and dipole–dipole interactions present here.

Introduction

Self-assembly of colloidal particles can be directed in various ways. For example, an external electric or magnetic field can change the symmetry of assembly of colloidal spheres if sufficient dipole–dipole interactions are induced.[1–3] Alternatively, one can vary the particle shape to achieve novel colloidal lattices.[4–7] Additionally, interparticle attractive and repulsive interactions can be adjusted to further tune the self-assembly process.

Significant progress in the fabrication of submicrometer- and micrometer-sized colloids in the past few years has yielded particles with complex colloidal shapes, such as rods,[8,9] platelets,[10] boards,[11,12] dumbbells,[13–15] cubes[16–21] and even peanuts.[22] The symmetries of their close packed structures have also been the focus of numerous investigations, as their self-assembled structures could lead to new functional materials.[1] An important aspect for the search of self-assembly using such anisotropic blocks is to ensure that interactions are well controlled.

Here, we investigate the organization of micron-sized cube-like hematite (α-Fe_2O_3) colloids with a permanent magnetic dipole[21–24] into three dimensional (3D) structures as a function of inter-cube interactions and external fields. The effect of particle shape, surface charge and alignment in a magnetic field on the resulting self-assembled structures is investigated. An important feature of these cubes is that their shape is best described by a superball, whose contour is represented by the formula:[25]

$$|x/a|^m + |y/a|^m + |z/a|^m = 1 \quad (1)$$

where m is the shape parameter, which indicates the extent of deformation from a sphere ($m = 2$) to a cube ($m = \infty$), a is half the edge length D. For superballs and similar shapes the phase behaviour has been recently determined theoretically and with computer simulation.[26–29] Experimental studies on nanometre-sized superballs have shown the continuous transformation of simple cubic to rhombohedral depending on m,[18] while for micron-sized superballs tunable depletion attraction resulted in simple cubic crystals[30] or convective drying into face centred cubic (FCC)-like stacking.[31] The two latter studies were done

[a]*Van 't Hoff Laboratory for Physical and Colloid Chemistry, Debye Institute for Nanomaterials Science, Utrecht University, Padualaan 8, 3584CH, The Netherlands. E-mail: A.V.Petukhov@uu.nl*

[b]*European Synchrotron Radiation Facility, 6 rue Jules Horowitz, BP 220, F-38043 Grenoble Cedex 9, France*

† Electronic supplementary information (ESI) available: Detailed information on the size and zeta potential measurements. Additional μrad-XRD patterns and/or profile plots of: hematite cubes in buffers, silica coated hematite cubes in water and ethanol, bare hematite cubes in a magnetic field, and differently sized silica coated hematite cubes in a magnetic field. Comparison of experimental lattice parameters with predicted densest packing from simulations. See DOI: 10.1039/c3sm51553b

‡ Current address: Department of Chemistry and Biochemistry, University of California Los Angeles, Los Angeles, California 90095, USA.

using an external driving force, *i.e.* depletion or capillary forces and convective flow.

In this study we made use of gravity, due to the large density of hematite, as a force to form sediments of hematite cubes. Because the cubes are charge stabilized, interactions were controlled by changing the dispersion medium, such as water and ethanol, and controlling the surface charge sign by changing pH or by coating the particles with a silica shell. Furthermore, the effects of an external magnetic field were investigated using specialized magnetic setups. Characterization of the formed structures was done using microradian X-ray diffraction (μrad-XRD) and focussing on the structural information obtained from the structure factor peaks. Using this approach, the most favourable conditions for the self-assembly of cubes into long-range ordered structures in the sediment were identified. An applied external magnetic field was used to induce particle alignment and the formation of a well-ordered crystal of silica coated hematite cubes. The formation of the sediment was imaged by Hard X-Ray Microscopy (HXRM) and showed that at the top of the fluid–solid interface a transformation from a rectangular symmetry to a hexagonal symmetry occurred, due to gravitational compression. The rectangular well-ordered single crystal was found to have a base centred monoclinic (BCM) symmetry, which rotates lower in the sediment due to the higher gravitational compression. Our investigation shows that controlled self-assembly of these sedimenting magnetic cubes can be achieved by controlling the interplay between magnetic dipole–dipole attraction and double layer repulsion.

Experimental

Materials

As solvents we used: deionized water from a Milli-Q water system (Millipore water, 18 MΩ cm), ethanol (100%, Fisher Chemicals), and ethanol (p.a. Merck). Synthesis of the hematite particles was performed using iron chloride hexahydrate (Sigma Aldrich), sodium hydroxide (Merck) in water and the silica coating with tetraethoxysilane (purum, >98% Fluka), and 0.25 wt% tetramethylammonium hydroxide solution (TMAH, Sigma Aldrich) in ethanol. Buffers were prepared from sodium bicarbonate (p.a. Merck), sodium carbonate (p.a. Merck), sodium acetate trihydrate (Lancaster, 99%), acetic acid (p.a. Merck), disodium hydrogen phosphate (Sigma Aldrich, >99%) and potassium dihydrogen phosphate (p.a. Merck) dissolved in water. All chemicals were used as received.

Cube synthesis

The synthesis of the colloidal hematite cubes was performed repeatedly with changing iron concentration to obtain hematite particles with various average edge lengths $\langle D \rangle$ between 500 and 1500 nm. The synthesis is well documented elsewhere.[16,21,32,33] In short, a 2 M $FeCl_3$ solution is mixed rapidly with a 6 M NaOH solution to form a gel–sol that is aged 8 days at 100 °C. The most crucial step in the preparation of the gel–sol is the precise moment at which the sodium hydroxide solution is added to the iron chloride solution. This step determines the number and quality of the precursor particles and is controlled by the addition speed, speed of stirring and temperature of the solution. When these factors are kept constant, the excess iron concentration determines the cube size. Therefore, syntheses were performed very accurately to improve the reproducibility of the cube size and shape. Silica coating occurred *via* an adaption of the Stöber method.[34] With this method a silica layer can be deposited on the hematite cubes.[30]

Particle characterization techniques

The particle shape and size were characterized by transmission electron microscopy (TEM, Philips TECNAI 10 or TECNAI 12). The zeta potential and size of the particles were determined using a Malvern Zetasizer Nanoseries by measuring very diluted dispersions in a disposable zeta-cuvette at 20 °C with an equilibration time of 120 s.

Sample preparation

The cubes were dispersed in different solvents: Millipore water (pH ∼ 5), ethanol, 6 mM TMAH in water (pH = 9) and 200 mM buffer; acetate buffer (pH = 3.6), phosphate buffer (pH = 5 and pH = 8) and carbonate buffer (pH = 9.2 and pH = 10.8). Cube dispersions of typically 5 wt% were placed in rectangular capillaries of 100 × 4 × 0.2 mm internal dimensions that were stored with their long axis parallel to the gravitational field. Sediments were obtained between 24 hours or 72 hours depending on the particle size. The sediments were inspected by eye for the presence of Bragg reflections.

Magnetic field setup

For magnetic field measurements we designed and manufactured two magnetic field setups consisting of six permanent magnets with the field oriented horizontally. The samples were placed at the centre of the magnetic field that could be adjusted between 20 mT and 600 mT. The first setup was used for screening the samples in a magnetic field for long periods of time. The second setup could be placed directly on the rotation and translation stage of beam-line 26B with correct centre-of-rotation positioning and sample rotations of ±70°. The results reported in this work are obtained with a magnetic field strength of 25 mT.

Microradian X-ray diffraction

Detailed information about the structure in the sediments was obtained by μrad-XRD using compound refractive lenses (CRL)[35–37] at beam-line 26B of DUBBLE[38–40] and μrad-XRD in combination with transmission HXRM at optics test bench ID06,[41,42] both at the ESRF in Grenoble. The selected energy for the X-ray beam was 13 keV for DUBBLE and 12.2 keV for ID06. The CCD X-ray detector used for μrad-XRD had a pixel size of 9 × 9 μm (Photonic Science). The detector was protected from the direct X-ray beam using a beam-stop with a wedge shape at DUBBLE (2 different occasions) and a bar shape at ID06. The HRXM detector was a high resolution CCD detector ESRF Frelon

2000 with a pixel size of 0.56 × 0.56 μm and dimensions of 2048 × 2048 pixels. The samples were placed between 6.7 and 7.5 m before the detectors. The X-ray beam size at the sample was 500 × 500 μm at DUBBLE and 200 × 200 μm at ID06. The sediments were scanned from top to bottom with the X-ray beam perpendicular to the flat side of the capillary. Rotation scans were performed around the sample vertical axis, ω, perpendicular to the X-ray beam.

Results & discussion

Cube properties

Of the synthesized variety of hematite cubes five were selected for sedimentation experiments based on their shape and/or low size polydispersity. The cube size and *m*-value, as determined from at least 100 individual particles in TEM images, are shown in Table 1, for selected cubes. The average cube edge lengths, $\langle D \rangle$, span a size range from 270 nm to 2085 nm. Four samples were selected for coating with silica and their sizes, shell thicknesses and *m*-values are also shown in Table 1. Fig. 1a–d show representative TEM images of the obtained hematite cubes with and without a silica coating, clearly showing the superball shape. Size measurements with dynamic light scattering were also performed but are challenging, due to the relatively high mass density of hematite (5.25 g cm^{-3}) that leads to fast sedimentation of the cubes. For more information see ESI.†

The gravitational length, a measure for the balance between thermal motion and gravitational transport, is given by $L_g = k_BT/M_bg$. Here k_BT is the thermal energy, M_b is the buoyant mass, and g is the gravitational acceleration. For the differently sized cubes, L_g is shown in the last column of Table 1. The L_g values are overall very small; the largest value is obtained for the smallest cubes but only extends over 10 particle dimensions and for larger cubes L_g is even similar to D. This indicates that sedimentation of the particles is unavoidable. Thus, dense sediments of the cubes will form, where gravitational compression will occur due to the mass of the cubes above.

Table 1 Particle properties of the hematite cubes and silica coated hematite cubes

Name	$\langle D \rangle$ (nm)	σ_D (%)	$\langle T_{SiO_2} \rangle$ (nm)	*m*	$L_{g\text{-}H_2O}$ (nm)
Fe_2O_3					
C15	269	17	—	[a]	5006
L2	533	4	—	3.60	641
V5	932	5	—	[a]	120
J1	1055	7	—	[a]	83
C9	2085	9	—	[a]	11
Fe_2O_3 + SiO_2					
C15_Si	340	13	33	[a]	2470
L2_Si	652	7	59	3.08	351
F1_Si	668	4	55	3.13	326
V5_Si	1028	4	48	3.55	89

[a] *m*-value not determined.

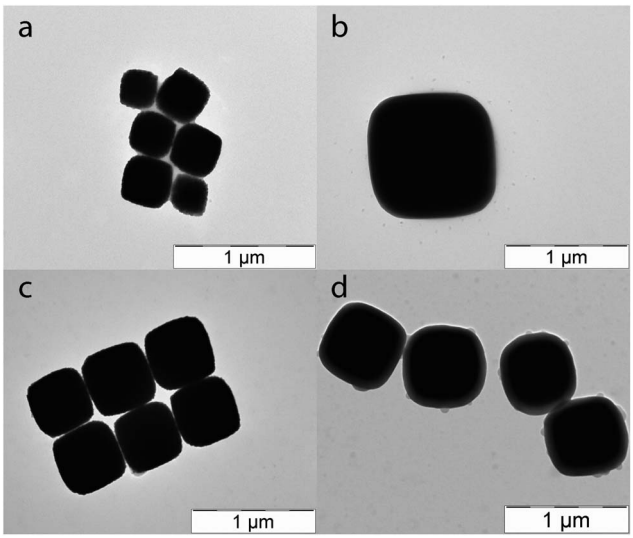

Fig. 1 TEM images of differently sized hematite cubes used for the experiments: (a) C15 with $D = 269$ nm, (b) V5_Si with $D = 1028$ nm, (c) L2 with $D = 533$ nm and (d) L2_Si with $D = 652$ nm. The '_Si' denotes that the cubes are coated with a silica shell. In the TEM images the shell can be seen as a light grey layer around the darker cores.

Hematite has an iso-electric point (IP) around 7.5–8.5.[43] In order to have a stable suspension we need to work either below or above the IP, to prevent aggregation due to van der Waals attraction with electrical double layer repulsion between the colloids. This changes when we coat the cubes with silica, because the point of zero charge changes to 1.7–3.5. In demineralized water the zeta potential of the L2 cubes is 38.2 mV while it changes to −48.5 mV for L2_Si, which is a reflection of the change of the point of zero charge. When we change the pH to 9 at low salt (6 mM TMAH in water) the value changes to −75.0 mV for L2, indicating the reverse of the charge sign above the IP (see ESI Table 1† for more details).

Hematite also possesses a magnetic moment (due to canted antiferromagnetism[21–24]) that induces dipole–dipole attractions. To obtain a stable self-assembling system of hematite cubes a balance between the van der Waals and magnetic attraction and the double layer repulsion has to be found.

Quantitative information on the pair interaction energy for the superballs in our study is at this stage scarce. The hematite cubes carry a magnetic moment that is clear from our results as well as from previous work.[21,23] However, the precise magnitude and orientation of the magnetic moment are still uncertain and the subject of on-going study.[21,44] With respect to the electrical double layer repulsion between the hematite and silica superballs it has to be realized that the accurate values of surface potentials or surface charge densities are difficult to obtain and zeta potentials cannot readily be converted into surface charge densities. For further discussion on this point we refer to ref. 45, which is an experimental study on the double layer interaction between charged silica spheres in ethanol. For the charged silica cubes in ethanol the pair interaction between two particles is further complicated by orientational dependence of both the double layer repulsion and the van der Waals attraction. For

example, the repulsion between two cubes in face-to-face orientation will be much larger than when the cubes approach each other facing their rounded edges. No theory or simulation results are available yet for the orientation-dependent DLVO interaction between two superballs. So here we have to restrict ourselves to a qualitative consideration based on the magnitude of the Debye length and the surface charge density.

The Debye screening length, κ^{-1}, is dependent on the dielectric constant, ε_r, and ionic strength, I, of the solvent according to: $\kappa^{-1} = \sqrt{(\varepsilon_0 \varepsilon_r k_B T / 2 N_A e^2 I)}$. In demineralized water with $\sim 10^{-5}$ M salt the Debye length is 97 nm and changes to 1 nm for 10^{-1} M salt. Changing the solvent by going from water $\varepsilon_r = 80$ to ethanol $\varepsilon_r = 20$ leads to a decrease in κ^{-1} from 97 nm to 49 nm.

Effect of pH and ionic strength on the sediment structure

Fig. 2 shows photographs of the sediments of differently sized bare hematite cubes in water, 6 mM TMAH (pH = 9) and water (pH ~ 3). It is interesting to see that the colour changes with hematite cube size, from bright orange to purple for C15 with D = 269 nm to J1 with D = 1055 nm, respectively. The cubes dispersed in water tend to adsorb on the capillary walls, indicating a strong interaction between the positive hematite surface and the negative glass surface. When the pH is elevated to 9 by the addition of TMAH the cubes, now being negatively charged, form clear sediments with weakly visible Bragg reflections. The largest (1 μm) cubes dispersed at pH ~ 3 show strong Bragg reflections, indicating that ordered structures have formed in the sediment.

In the 2D microradian X-ray patterns of the bare hematite cubes in different solvents, interesting features were observed revealing short-range as well as long-range order. The scattering patterns are of course influenced both by the form factor and structure factor. In order to disentangle these effects we would have to subtract a measured form factor of a hematite cube. However, the required measurement on dilute cubes in bulk dispersions is unfeasible due to rapid cube sedimentation. Moreover, the non-spherical shape couples the orientational and positional interparticle correlations making the form and structure factor separation ambiguous. Therefore, we limit ourselves to analysis of the structure factor peaks, which can be clearly distinguished in most of the μrad-XRD patterns. In the height scans along the samples, order could often be observed over a range of a few mm in typically 5 mm high sediments. The bottom of the sediments usually showed less order, due to the gravitational compression exerted by the total mass of the cubes above causing kinetic arrest. Furthermore, samples containing polydisperse particles showed size fractionation that affected the formed structures.

In Fig. 3(a)–(c) we show typical 2D μrad-XRD patterns of hematite cube L2 sediments with D = 533 nm dispersed in, Millipore water, 200 mM carbonate buffer (pH 9.2) and 6 mM TMAH in water (pH 9) taken at 1 mm from the top of the sediment. The black wedge is the shadow of the beamstop that protects the detector from the direct X-ray beam. For hematite cubes in demineralized water (Fig. 3a) a strong structure factor peak can be observed at q = 0.0110 nm^{-1} on top of the form factor (for profile see ESI Fig. 2†), indicating that the hematite cubes positions are locally correlated. The presence of a ring indicates that the sample is very polycrystalline and order extends over roughly 5–10 cube lengths. The d spacing of

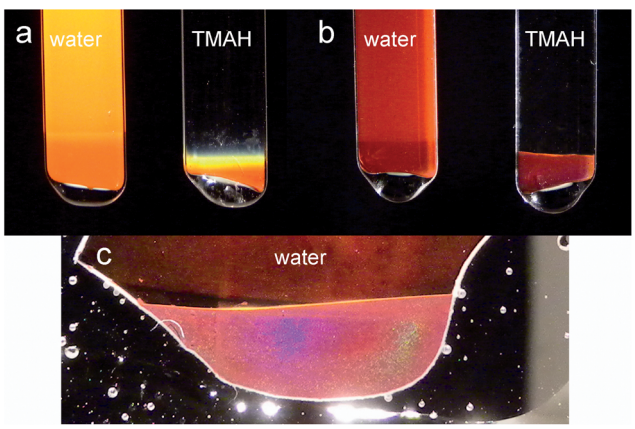

Fig. 2 Photographs of the sediments obtained in dispersions of the different hematite cubes (a) C15 with D = 269 nm, (b) L2 with D = 533 nm in water and in water with pH 9 by the addition of TMAH and (c) J1 with D = 1055 nm in water pH 3. Note the color change of the hematite from orange to purple with increasing particle size. Adsorption of the hematite cubes to the glass walls is observed in water, due to the opposite charges of their surfaces. At pH 9 (6 mM TMAH in water) the surface charges are both negative and clear sediments are obtained. At pH ~ 3 the large cubes still adsorb slightly, however, due to a higher surface charge, a clear sediment is also obtained.

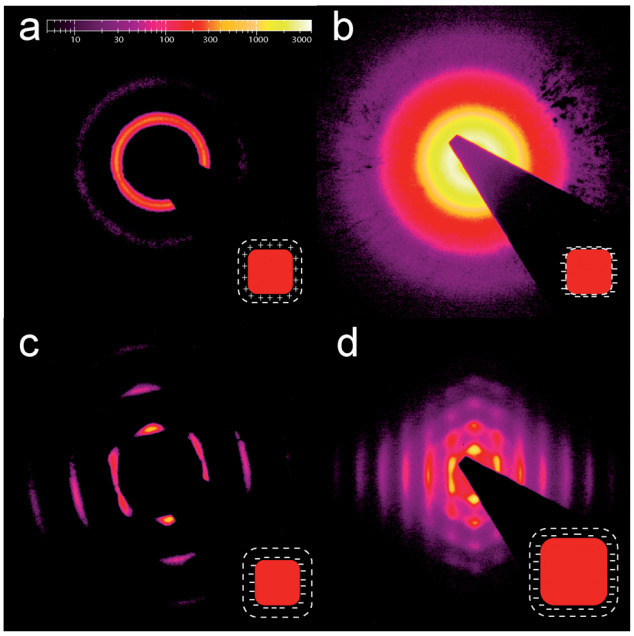

Fig. 3 2D μrad-XRD patterns of the sediment of hematite cubes L2 with D = 533 nm in different solvents: (a) Millipore water, (b) 200 mM phosphate buffer, pH 9.2 and (c) 6 mM TMAH, pH 9; (d) 2D μrad-XRD pattern of cube J1 with D = 1055 nm at pH ~ 3. Single crystal structures are seen for L2 and J1 at high surface charge. The insets show schematic representations of the cube charges and changing Debye length. The black wedge is the shadow of the beamstop to protect the detector from the direct X-ray beam.

571 nm shows that the cubes are not aligned perfectly side-to-side but have a slightly rotated orientation with respect to their neighbors. The short-range order can be explained by the low surface charge density the hematite particles carry in water.[46] The magnetic attractions cause the cubes to form small flexible strings that will cluster and form small crystallites that sediment with different orientations.[21,23,44] However, once in the sediment the surface charge is not high enough to compensate the gravitational compression causing kinetic arrest and an inability for neighboring crystals to reorient.

For cubes dispersed in 200 mM buffer with pH 9.2 aggregation of the particles was observed during preparation and a larger sediment was obtained than for cubes dispersed in water at the same wt%. The μrad-XRD pattern of this sample is dominated by a weak form factor and no clear structure factor peak can be observed (Fig. 3b and ESI Fig. 2d†). This shows that little correlation between cube positions is present. The high salt content of the buffer decreases κ^{-1} to >1 nm and destabilizes the cubes such that they irreversibly aggregate upon string formation due to the van der Waals forces. The formation of these random clusters of cubes results in loosely packed, low density sediments.

For cubes that are dispersed in 6 mM TMAH in water at pH 9, the surface charge sign is reversed and κ^{-1} is reduced to 4 nm. However, the addition of TMAH causes additional surface charges by the adsorption of $[(CH_3)_4N]^+$ cations on the cube surface.[46,47] The μrad-XRD pattern shows the presence of a large single crystal domain (Fig. 3c) indicating that these conditions are favorable for structure formation. The observed Bragg spots indicate that the crystal orientation is extended over at least 500 × 500 μm (the X-ray beam size). The two almost vertical peaks, at $q = 0.0111$ nm^{-1}, indicate that layers of cubes with a *d*-spacing of 566 nm have formed perpendicular to the direction of the gravitational field. This is quite understandable as intra-layer ordering of the cubes will likely favor alignment of the cubes flat sides. Furthermore, the flat walls and bottom of the capillary will most likely also induce directionality due to cube alignment. The two horizontally smeared peaks, at $0.0115 < q < 0.0117$ nm^{-1}, indicate that the layers of cubes are randomly shifted on top of each other resulting in periodic distances of 546–537 nm. Cubes in a layer above are dominantly positioned in the niches formed by two cubes below (brick-wall-like), resulting in the two hexagonal peaks. However, the cube positions in the layers can also be on top of each other resulting in a horizontal peak.

The formation of long range ordered crystalline structures for cubes dispersed in water at pH 9 with TMAH and only short-range order in demineralized water is explained by a higher surface charge on the cubes. Hematite has a relatively low surface charge in water and the addition of TMAH increases the surface charge,[46,47] as manifested by the found distance of 566 nm between the cube sides with $D = 533$ nm for the TMAH sample. Thus, by tuning the hematite surface charge and salt concentration, the formation of long-range crystal structures can be controlled during sedimentation. The obtained layered crystal structure is induced by the cube shape and attractive magnetic interactions.

That a high surface charge is the origin of the higher order is confirmed by the presence of a similar 2D μrad-XRD pattern with hexagonal peaks obtained in the sediment of 1055 nm cubes at pH 3 (Fig. 3d). The cubes can, surprisingly, form a similar ordered structure under these high surface charge conditions despite having a very fast sedimentation time (~7 hours for 8 cm). For the biggest cubes C9 with $D = 2085$ nm no ordered structures were observed, indicating that sedimentation is too fast to allow organization of these large cubes in the sediment.

We realize that the explanations of the various structures presented above still lack a quantitative basis. Though we know Debye lengths and have an estimate of the zeta potential the details of the double layer repulsion between the cubes are still unknown. There is still no expression for the anisotropic DLVO potential between two spheres, in addition the magnitude and direction of the magnetic moment is still under study. So clearly computer simulation of sedimentary crystals of cubes would be very helpful in further quantitatively explaining our findings.

Silica coating and solvent effect on the sediment structure

Fig. 4 shows photographs of sediments of silica coated hematite cubes with a negative surface charge in different solvents. The main difference in behavior is observed between water and ethanol samples. While having a similar surface charge of −50 and −57 mV in ethanol and water respectively, the particle behavior is quite different. The cubes dispersed in water are slightly adsorbed onto the glass wall, while those dispersed in ethanol do not show signs of adsorption and reveal distinct Bragg reflections in the sediment, indicating ordering of the cubes.

In Fig. 5 the 2D μrad-XRD patterns of the silica coated hematite cubes L2_Si, with a 652 nm edge length, dispersed in water and ethanol are shown. In water silica-coated cubes (Fig. 5a) show the same ordering as that observed for the bare hematite cubes in water (Fig. 3a). A strong but broad structure factor ring is present indicating local short-range order of the cubes. For the cubes in ethanol a single pattern is observed revealing the presence of long-range order (Fig. 5b), as the hexagonally ordered Bragg peaks can be observed up to the third order.

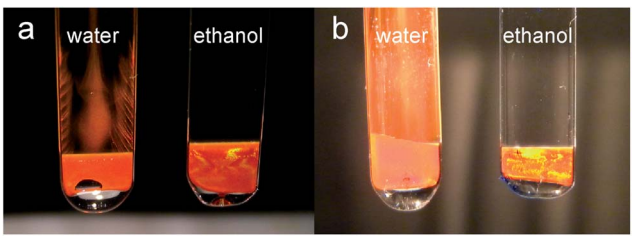

Fig. 4 Photographs of the sediments of silica coated hematite cubes (a) C15_Si with $D = 340$ nm and (b) L2_Si with $D = 652$ nm dispersed in water and ethanol. Cubes dispersed in water adsorb slightly onto the glass wall, while strong Bragg reflections are visible for the cubes dispersed in ethanol, indicating ordering in the sediments.

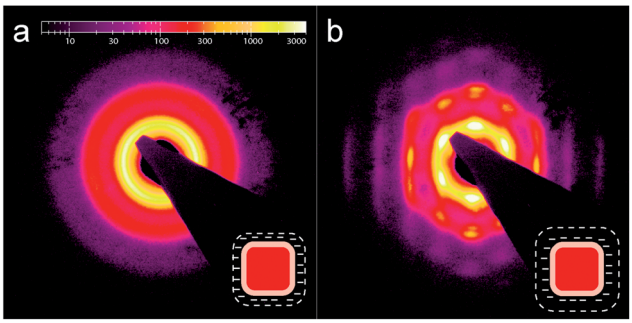

Fig. 5 2D μrad-XRD patterns of silica coated hematite cubes L2_Si with D = 652 nm in (a) water and (b) ethanol. In water only short-range local order is observed, while in ethanol long-range ordered single crystal structures are obtained, due to higher screening of the double layer repulsion in water.

In the ethanol case, the cubes have also ordered into layers that are oriented perpendicular to the gravitational field. However, the six peaks indicate that much more positional correlations exist between the layers, with the "brick-wall" stacking dominating. The intensity of the two horizontal peaks is slightly smeared, indicating that the layers are not always perfectly ordered and it is clear that the square orientation is much less present.

The difference in sediment structure between water and ethanol as a dispersion medium originates from the difference in screening of the double layer repulsion. Although both the Millipore water and ethanol should contain a low electrolyte concentration, it is known that silica can dissociate in water[31] and thus the salt concentration is raised in water which decreases κ^{-1} in this case. The profile plots along the Bragg spots also show that the cubes in water are located at much closer distances than the cubes in ethanol, indicating a longer ranged repulsion between the silica coated cubes in ethanol (ESI Fig. 3†).

Thus, by tuning the interactions between the cubes with an additional silica layer a crystal with extended long-range order can be formed. This can be explained by a higher surface charge. However, the presence of a silica layer can also affect the magnetic attraction, as the inter-particle distance of weakly magnetic hematite cube centers is increased. This decreases the magnetic attraction of the hematite cores and allows the particles to align better.

Effect of cube size on the sediment structure

To determine whether the observed crystal structure is a result of the cube shape and the magnetic inter-cube interactions, the effect of cube size was also investigated. Simulation studies and experiments have already shown a correlation between the superball m-value, which changes with cube size and coating,[21] and the expected crystal structure.[25–28]

Differently sized cubes were coated with silica and dispersed in ethanol. Similar structures were observed in the sediments of smaller and larger cubes than L2_Si. In Fig. 6 the 2D μrad-XRD patterns are shown for the sediments of C15_Si, D = 340 nm (Fig. 6A), F1_Si, D = 667 nm (Fig. 6b) and V5_Si, D = 1028 nm (Fig. 6C) silica coated cubes in ethanol. For the F1_Si cubes, of similar size to L2_Si, the same pattern is observed and hence the same crystal structure is formed. It is also clear that for cubes of much smaller size, C15_Si, and much larger, V5_Si, the same hexagonal order and layering can be observed. However, for the smaller cubes less order is found (Fig. 6a), which is probably the result of the high polydispersity, 13%, which is known to hinder crystallization. For the bigger cubes, the faster sedimentation is probably the cause of the lower long-range order as also found for the bare hematite cubes (Fig. 6c). In Fig. 6d a schematic representation of the hexagonal stacked layers of cubes is shown. Here the dashed lines indicate the periodic hexagonal order between the layers. Clearly, the cube shape and dipole–dipole interactions determine the crystal structure as for all sizes a similar layered crystal structure is obtained. To see to what extent m plays a role, more detailed investigation is needed.

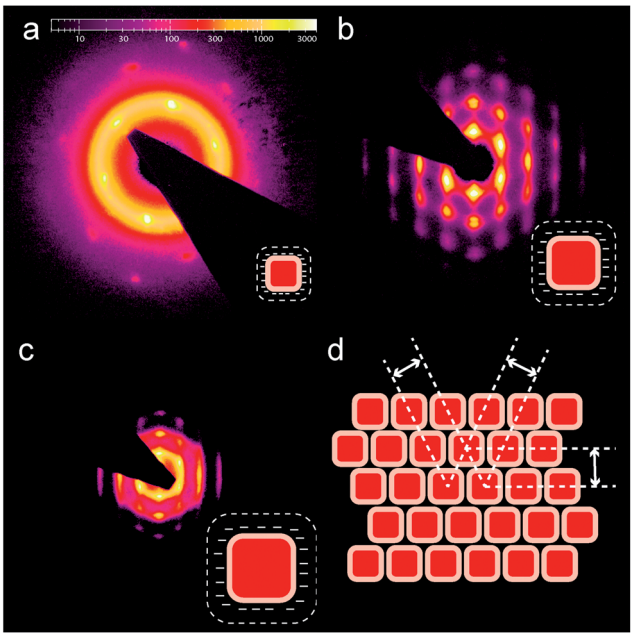

Fig. 6 2D μrad-XRD patterns of the sediments of silica coated hematite cubes of different sizes (a) C15_Si with D = 340 nm, (b) F1_Si with D = 667 nm and (c) V5_Si with D = 1028 nm. All patterns show distinct hexagonal Bragg peaks indicating layered ordering with a brick-wall-like layered stacking induced by the cube shape. (d) A schematic representation of the layered structure, showing the origin of the hexagonal peaks.

Effect of an external magnetic field – directed assembly

Because the hematite cubes possess a permanent magnetic dipole, we explored inducing directionality into the sediments of the hematite cubes with an external magnetic field. It was found that the best results were obtained when the sediments were redispersed using manual shaking and ultrasonic radiation for ~15 min, after that the particles were allowed to settle in a magnetic field of 25 mT. This process allows the cubes to align their magnetic moment to the magnetic field while sedimenting.

The 2D μrad-XRD patterns of the sediment of bare hematite cubes dispersed in 6 mM TMAH in water in an applied magnetic

field showed a cubic form factor but no Bragg peaks were observed (ESI Fig. 4†). The 2D form factor indicates that all cubes acquired the same orientation in the magnetic field. However, the lack of Bragg peaks suggests that under these conditions the cubes get jammed during sedimentation. The magnetic field probably induces strong inter-cube attractions inducing string and cluster formation that sediment faster than single particles causing the jamming.

Silica coated hematite cubes in ethanol are known to be stable in an applied magnetic field.[21] Rossi *et al.* showed that at low volume fractions string formation occurs and at higher concentrations large square ordered rectangular 2D domains form.[21] However, as optical light microscopy was used, these studies were limited to single layers of cubes and thus the analysis to 2D structures. Due to the high penetration depth of the X-rays, the 200 μm thick samples can easily be studied with a combination of μrad-XRD and HRXM. The beam-size of the used setup at ID06 is 200 × 200 μm allowing a more detailed investigation of the sediments than the setup at DUBBLE.

Full scans of the sediments of silica coated hematite cubes sedimented at 25 mT revealed large single crystalline structures with long-range order in the sediment. Furthermore, an interesting structural change was observed at the fluid–solid interface. In Fig. 7(a)–(c) three 2D μrad-XRD patterns of the fluid–solid interface at $z = 0$ of the sediment of L2_Si are shown (for C15_Si and F1_Si see ESI Fig. 5†). An isotropic pattern is obtained just above the sediment (Fig. 7a), while clear Bragg peaks with rectangular (Fig. 7b) and hexagonal (Fig. 7c) symmetry are observed in the two patterns at and below the interface at $z = -0.1$ mm and $z = -0.9$ mm, respectively. In Fig. 7(d)–(g) HRXM images of the interface are shown. In Fig. 7d the transition region from a fluid region to an ordered region with a slightly tilted square structure can be clearly seen. This square structure shows very strong resemblance to the square structures observed by light microscopy.[21] However, here the image is a transmission of >300 cubes which are perfectly ordered along the X-ray beam. From the HRXM images the height of the square region was determined to be around 100 μm; after that the order disappears (Fig. 7f) and shifts to hexagonal lower in the sediment (Fig. 7g). The formation of the sediment could be followed over time and the square region was found to always remain around 100 μm high and persisting over the full width, 4 mm, of the capillary.

To understand what is happening at the interface rotation scans of the sediment in the square and hexagonal regions were performed over a range of ±70° with 1° or 5° steps. These measurements were again performed with a 500 × 500 μm beam at DUBBLE, thus an overlap of the square and hexagonal region was unavoidable. μrad-XRD patterns of significant angles taken from the rotation scans are shown in Fig. 8; at these angles the strongest Bragg peaks were observed.

In the 2D μrad-XRD patterns of the top region of the sediment at $z = -0.1$ Bragg spots with square symmetry can be observed at $\omega = -40°$, 0° and 45°, indicating a cubic type crystal lattice. At −40° and 45° the Bragg peaks are even visible up to the 10th order (out of the range of Fig. 8a and e) indicating that

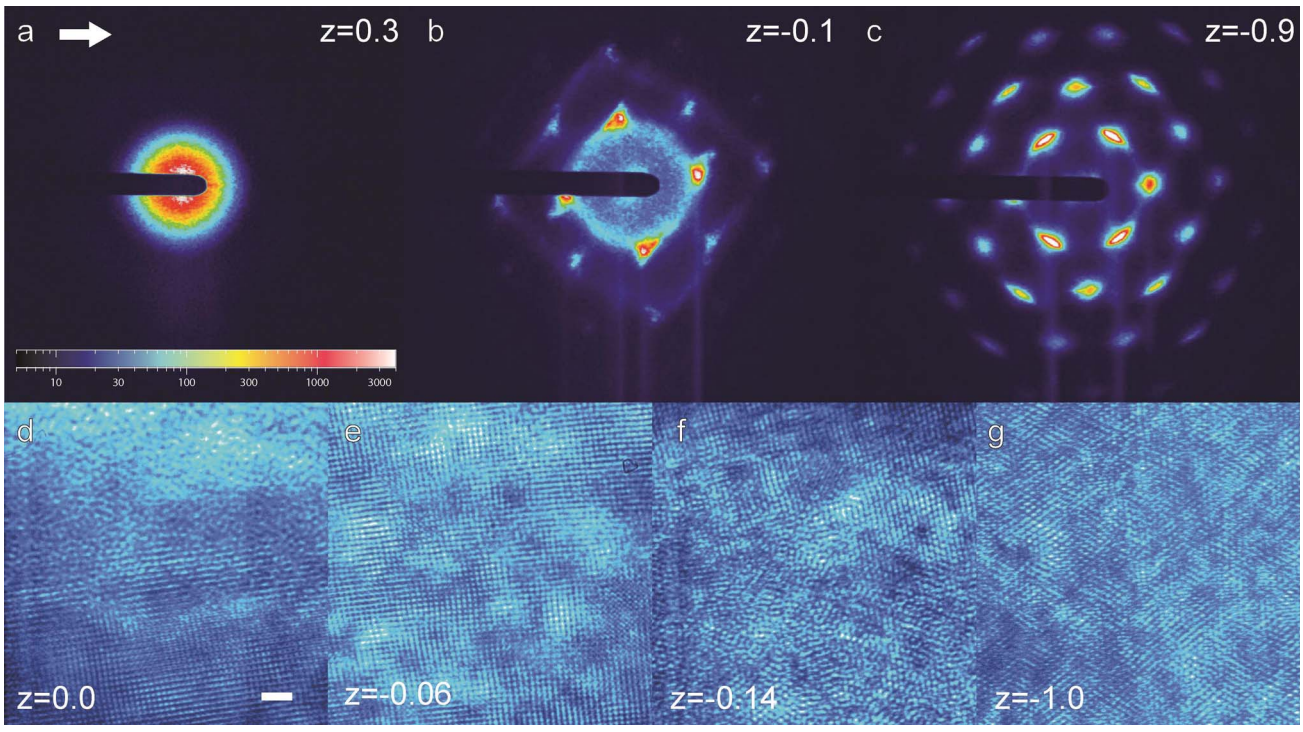

Fig. 7 μrad-XRD patterns (a–c) and HXRM images (d–g) of the sediment of L2_Si cubes with $D = 652$ nm in a 25 mT magnetic field after 12 hours, taken around the fluid–solid interface, $z = 0$, of the sediment. Different structures are formed at these positions with rectangular and hexagonal periodicity perpendicular to the X-ray beam. The large white arrow in (a) indicates the direction of the B-field, the scale bar in (d) is 3 μm.

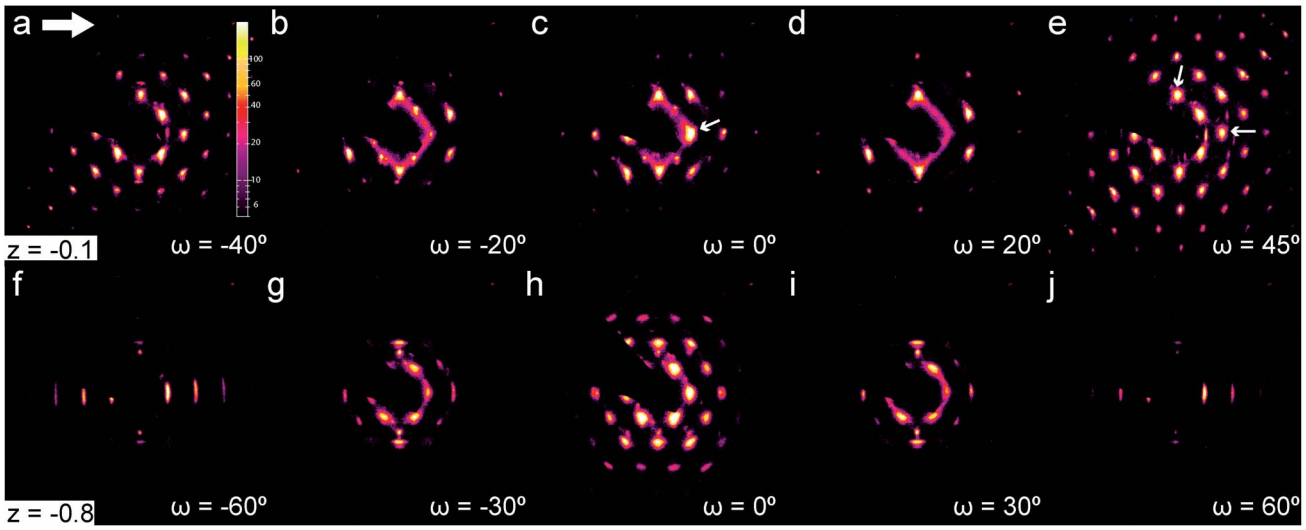

Fig. 8 μrad-XRD patterns obtained with X-ray beam orthogonal to the sediment ($\omega = 0°$) of L2_Si in a 25 mT magnetic field, after a sample rotation around the vertical axis ω; (a–e) for the top of the sediment at $z = -0.1$ mm, the large white arrow in (a) indicates the direction of the B-field and (f–j) for the middle of the sediment at $z = -0.8$ mm. In the top region strong Bragg peaks with square symmetry are visible up to high orders, indicating a well ordered single crystal of cubes. In the lower part hexagonal peaks are observed up to $\omega = \pm 35°$. For $\omega > 35°$ smeared peaks are present, indicating that this structure is less ordered.

this structure is very well ordered. In the hexagonal region at $z = -0.8$, the strong hexagonal Bragg spots are observed up to $\omega = 35°$. For $\omega > 35°$ smeared peaks in the horizontal direction can be observed together with some weak contributions of the Bragg spots of the cubic region. The hexagonal structure lower in the sediment possesses less order than the cubic structure at the interface. Clearly, the gravitational compression plays an important role here.

To determine the exact crystal lattice, first the positions of the Bragg peaks were determined for the top region of the sediment. The two vertical peaks observed in the patterns at $q = 0.0129$ nm^{-1} were found to be present for each rotation ω, indicated with the top arrow in Fig. 8e. This shows that there are crystal lattice planes, spaced by 486 nm, that are oriented perpendicular to the beam and parallel to the field. We can therefore deduce that the magnetic field induced directionality of planes along the field. The additional horizontal peaks (right arrow, Fig. 8e) at $q = 0.0147$ nm^{-1} at $\omega = -40°$ and $q = 0.0149$ nm^{-1} at $\omega = 45°$ show that the cubic lattice horizontal lattice planes are present with a slightly different spacing of 426 and 423 nm. At $\omega = 0°$ the horizontal peak is located at $q = 0.0111$ nm^{-1} giving a spacing of 566 nm. From the symmetry the structure can be identified as an FCC-like structure with the [100] projections (Fig. 8a and e) and [110] (Fig. 8c) seen over 90° of rotation. However, the rotation between the [100] structures is only 85° and therefore the structure is identified as a Base Centered Monoclinic (BCM) lattice, with lattice parameters of $a = 846$ nm, $b = 852$ nm and $c = 972$ nm with $\alpha = \beta = 90°$ and $\gamma = 85°$.

Simulations have also predicted FCC-type lattices, namely the C_0 and C_1 lattice for superballs[25] and a sheared FCC or sheared SC for parallel rounded cubes.[28] The experimental BCM structure was therefore compared to the crystal structures predicted by simulations. For this we calculated the expected BCM lattice parameters that are also present in an FCC-type lattice in 3 orientations for $m = 3.08$. We could not find an exact fit of our experimental BCM lattice with any of the calculated simulation BCM lattices (see ESI Table 2†). This can be explained by the fact that in the simulations only excluded volume interactions were taken into account, while here long-range repulsive forces and dipole–dipole interactions play an important role.

To completely understand the BCM structure, the orientation of the cubes on the lattice should also be determined. From earlier investigations of the cube internal structure it was determined that the orientation of the magnetic dipole is oriented perpendicular to the long diagonal of the cube.[21,48] So, to which cube sides the dipole moment points exactly and how the cube will align in the magnetic field has not been established. It is, however, clear that the layers aligned parallel to the magnetic field are spaced further apart than the layers arranged vertically and thus we can conclude that the long-diagonal of the cubes is oriented perpendicular to the field.

The hexagonal crystal structure lower in the sediment was actually found to correspond to the identified BCM lattice above but with a 30° rotation backward or forward along the X-ray beam at 0°. In this orientation the flat sides of the cubes are parallel to the capillary bottom. This crystal structure is explained as follows. The total buoyant mass of the crystal above is exerting a large pressure on the bottom part. The cubes are aligned with their long diagonal perpendicular to the field; however, as seen for the other crystals in a gravitational field, the cubes preferably align with their flat sides to the capillary wall and bottom. Apparently the high pressure exerted by 100 μm of the sediment is enough to overcome the magnetic dipole alignment and to induce a flat alignment of the cube sides again.

To summarize, the alignment of hematite cubes in a magnetic field causes the formation of a BCM crystal lattice.

First the randomly oriented cubes align their magnetic dipole moment in the applied magnetic field. Then, due to sedimentation, the cubes pack into a closely packed crystal structure, still with their magnetic dipole aligned. As the structure builds, more and more pressure is exerted on the structure below, and the structure rotates such that the flat sides of the cubes orient parallel to the capillary wall and bottom. This results in a slight loss of positional correlation of the BCM structure.

Conclusions

Self-assembly of colloidal hematite cubes in sedimentary crystals can be controlled by a number of factors, such as solvent, coating, size and external field. The mechanism governing the self-assembly is an interplay between the cube shape, the magnetic dipole–dipole attraction and surface charge repulsion. Short-range ordered structures were obtained for hematite cubes at low surface charge, while at higher surface charge the cubes were found to form long-range ordered layered crystal structures, due to the cube shape. Aggregation was observed for samples at high salt concentration that reduces the Debye length dramatically. Single crystals with long-range order were obtained for silica coated hematite cubes dispersed in ethanol, a low dielectric solvent that provides long range repulsion between the cubes. The cube size was found to have a small effect as the same crystal structures were obtained.

For silica coated hematite cubes, directionality of the crystal structures was induced with an external magnetic field. Single crystalline structures with a BCM crystal structure were obtained for the first 100 μm of the sediment. Here the cubes are aligned with their magnetic dipole moment in the field. Below this the crystal structure is condensed under its own buoyant mass and the crystal structure was found to rotate 30°, which allows the cubes to orient with their flat sides aligned to the capillary wall and bottom. The found structure does not correspond to those predicted by simulations, due to the presence of dipole–dipole interactions and long-range repulsion between the cubes here.

In future experiments we plan to investigate the phase behaviour of these silica coated hematite cubes in more detail to address the full phase behaviour and determine how it compares to the phases predicted by simulations for the superballs.[27,28]

Acknowledgements

We would like to thank the Netherlands Organization for Scientific Research (NWO) and the European Synchrotron Radiation Facility (ESRF) in Grenoble for the provided beamtime. G. Portale and D. Detolenaire form BM26 and C. Detlefs and T. Roth from ID06 are thanked for their support during the measurements. For their assistance and input during the measurements we gratefully thank J. Hilhorst, A. B. G. M. Leferink op Reinink and M. Vis. For contributions to the syntheses S. I. R. Castillo, V. Meester, L. Pompe, J. W. J. de Folter and F. H. Hagemans are thanked. W. T. M. Irvine is thanked for providing the *m*-value analysis MatLab scripts.

Notes and references

1 A. Yethiraj and A. van Blaaderen, *Nature*, 2003, **421**, 6922.
2 V. Malik, A. V. Petukhov, L. He, Ya. Yin and M. Schmidt, *Langmuir*, 2012, **28**, 14777–14783.
3 Q. Zhang, M. Janner, L. He, M. Wang, Y. Hu, Y. Lu and Y. Yin, *Nano Lett.*, 2013, **13**, 1770–1775.
4 A. van Blaaderen, *Nature*, 2006, **439**, 7076.
5 S. C. Glotzer and M. J. Solomon, *Nat. Mater*, 2007, **6**, 557–562.
6 S. M. Yang, S.-H. Kim, J.-M. Lim and G.-R. Yi, *J. Mater. Chem.*, 2008, **18**, 2177–2190.
7 P. F. Damasceno, M. Engel and S. C. Glotzer, *Science*, 2012, **337**, 6093.
8 A. Kuijk, D. V. Byelov, A. V. Petukhov, A. van Blaaderen and A. Imhof, *Faraday Discuss.*, 2012, **159**, 181–199.
9 M. P. B. van Bruggen, F. M. van der Kooij and H. N. W. Lekkerkerker, *J. Phys.: Condens. Matter*, 1996, **8**, 9451–9456.
10 F. M. van der Kooij, K. Kassapidou and H. N. W. Lekkerkerker, *Nature*, 2000, **406**, 6798.
11 E. van den Pol, A. V. Petukhov, D. M. E. Thies-Weesie, D. V. Byelov and G. J. Vroege, *Phys. Rev. Lett.*, 2009, **103**, 258301.
12 E. van den Pol, A. V. Petukhov, D. M. E. Thies-Weesie, D. V. Byelov and G. J. Vroege, *J. Colloid Interface Sci.*, 2010, **352**, 354–358.
13 I. D. Hosein, B. S. John, S. H. Lee, F. A. Escobedo and C. M. Liddell, *J. Mater. Chem.*, 2009, **19**, 344–349.
14 A. F. Demirors, P. M. Johnson, C. M. van Kats, A. van Blaaderen and A. Imhof, *Langmuir*, 2010, **26**, 14466–14471.
15 D. J. Kraft, R. Ni, F. Smallenburg, M. Hermes, K. Yoon, D. A. Weitz, A. van Blaaderen, J. Groenewold, M. Dijkstra and W. K. Kegel, *Proc. Natl. Acad. Sci. U. S. A.*, 2012, **109**, 10787–10792.
16 T. Sugimoto and K. Sakata, *J. Colloid Interface Sci.*, 1992, **152**, 2.
17 F. Li, S. A. Delo and A. Stein, *Angew. Chem., Int. Ed.*, 2007, **46**, 6666–6669.
18 Y. Zhang, F. Lu, D. van der Lelie and O. Gang, *Phys. Rev. Lett.*, 2011, **107**, 135701.
19 S. A. Disch, E. Wetterskog, R. P. Hermann, G. Salazar-Alvarez, P. Busch, T. Brueckel, L. Bergstroem and S. Kamali, *Nano Lett.*, 2011, **11**, 1651.
20 H. Chan, A. Demortiere, L. Vukovic, P. Kral and C. Petit, *ACS Nano*, 2012, **6**, 4203–4213.
21 L. Rossi, Colloidal Superballs, PhD thesis, Utrecht University, The Netherlands, 2012.
22 S. H. Lee and C. M. Liddell, *Small*, 2009, **5**, 1957–1962.
23 M. Ozaki, H. Suzuki, K. Takahashi and E. Matijevic, *J. Colloid Interface Sci.*, 1986, **113**, 76–80.
24 N. K. Chaudhari, H. C. Kim, C. S. Kim, J. Park and J.-S. Yu, *CrystEngComm*, 2012, **14**, 2024–2031.
25 Y. Jiao, F. H. Stillinger and S. Torquato, *Phys. Rev. E: Stat., Nonlinear, Soft Matter Phys.*, 2009, **79**, 041309.
26 R. D. Batten, F. H. Stillinger and S. Torquato, *Phys. Rev. E: Stat., Nonlinear, Soft Matter Phys.*, 2010, **81**, 061105.
27 R. Ni, A. P. Gantapara, J. de Graaf, R. van Roij and M. Dijkstra, *Soft Matter*, 2012, **8**, 8826.

28 M. Marechal, U. Zimmermann and H. Löwen, *J. Chem. Phys.*, 2012, **136**, 144506.
29 F. Smallenburg, L. Filion, M. Marechal and M. Dijkstra, *Proc. Natl. Acad. Sci. U. S. A.*, 2012, **109**, 17886–17890.
30 L. Rossi, S. Sacanna, W. T. M. Irvine, P. M. Chaikin, D. J. Pine and A. P. Philipse, *Soft Matter*, 2011, **7**, 4139–4142.
31 J. M. Meijer, F. Hagemans, L. Rossi, D. V. Byelov, S. I. R. Castillo, A. Snigirev, I. Snigireva, A. P. Philipse and A. V. Petukhov, *Langmuir*, 2012, **28**, 7631–7638.
32 T. Sugimoto, M. M. Khan, A. Muramatsu and H. Itoh, *Colloids Surf., A*, 1993, **79**, 233–247.
33 T. Sugimoto, Y. S. Wang, H. Itoh and A. Muramatsu, *Colloids Surf., A*, 1998, **134**, 265–279.
34 C. Graf, D. L. J. Vossen, A. Imhof and A. van Blaaderen, *Langmuir*, 2003, **19**, 6693–6700.
35 A. Snigirev, V. Kohn, I. Snigireva and B. Lengeler, *Nature*, 1996, **384**, 6604.
36 V. Kohn, I. Snigireva and A. Snigirev, *Opt. Commun.*, 2003, **216**, 247–260.
37 M. Drakopoulos, A. Snigirev, I. Snigireva and J. Schilling, *Appl. Phys. Lett.*, 2005, **86**, 014102.
38 E. Homan, M. Konijnenburg, C. Ferrero, R. E. Ghosh, I. P. Dolbnya and W. Bras, *J. Appl. Crystallogr.*, 2001, **34**, 519–522.
39 A. V. Petukhov, J. H. J. Thijssen, D. C. 't Hart, A. Imhof, A. van Blaaderen, I. P. Dolbnya, A. Snigirev, A. Moussaid and I. Snigireva, *J. Appl. Crystallogr.*, 2006, **39**, 137–144.
40 J. H. J. Thijssen, A. V. Petukhov, D. C. 't Hart, A. Imhof, C. H. M. van der Werf, R. E. I. Schropp and A. van Blaaderen, *Adv. Mater.*, 2006, **18**, 1662.
41 A. Bosak, I. Snigireva, K. S. Napolskii and A. Snigirev, *Adv. Mater.*, 2010, **22**, 3256.
42 D. V. Byelov, J. M. Meijer, A. Snigirev, I. Snigireva, L. Rossi, A. Kuijk, A. P. Philipse, A. Imhof, A. van Blaaderen, G. J. Vroege and A. V. Petukhov, *RSC Adv.*, 2013, **3**, 15670.
43 L. Cromières, V. Moulin, B. Fourest and E. Giffaut, *Colloids Surf., A*, 2012, **202**, 101–115.
44 A. I. Abrikosov, S. Sacana, A. P. Philipse and P. Linse, *Soft Matter*, 2013, **9**, 8904–8913.
45 A. P. Philipse and A. Vrij, *J. Chem. Phys.*, 1988, **88**, 6459.
46 S. Sacana, L. Rossi and A. P. Philipse, *Langmuir*, 2007, **23**, 9974–9982.
47 Â. L. Andrade, J. D. Fabris, J. D. Adrisson, M. A. Valente and J. M. F. Ferreira, *J. Nanomater.*, 2012, 454759.
48 G. S. Park, D. Shindo, Y. Waseda and T. Sugimoto, *J. Colloid Interface Sci.*, 1996, **177**, 198–207.